Available online at www.sciencedirect.com
ScienceDirect
Trans. Nonferrous Met. Soc. China 33(2023) 409−421
Transactions of Nonferrous Metals Society of China
www.tnmsc.cn

Enhancing mechanical properties and degradation performance of Mg−0.8wt.%Ca alloy by directional solidification

Yi ZHANG[1,2], Xiao-hui FENG[1], Qiu-yan HUANG[1], Ying-ju LI[1], Yuan-sheng YANG[1,2]

1. Institute of Metal Research, Chinese Academy of Sciences, Shenyang 110016, China;
2. School of Materials Science and Engineering, University of Science and Technology of China, Shenyang 110016, China

Received 8 October 2021; accepted 31 December 2021

Abstract: The mechanical properties and degradation performance in Hank's solution of the directionally solidified (DSed) Mg−0.8Ca (wt.%) alloys were investigated and compared with those of the as-cast alloy. The microstructure was studied by OM, SEM, TEM, and EBSD. It is found that the columnar grains in DSed alloys have a consistent growth orientation of $\langle 11\bar{2}0\rangle$. The mechanical strength and ductility of Mg−0.8Ca alloy are significantly improved after directional solidification. Besides, the corrosion resistance of Mg−0.8Ca alloy in Hank's solution is dramatically enhanced after directional solidification. The Mg−0.8Ca alloys in Hank's solution mainly undergo microgalvanic corrosion, and the corrosion products consist of $Mg(OH)_2$, $(Ca,Mg)_3(PO_4)_2$, and hydroxyapatite (HA). The superior properties of the DSed Mg−Ca alloy are beneficial from the columnar microstructure and the redistribution of the eutectics. The DSed Mg−0.8Ca alloy with columnar dendritic structure is expected to be used as biodegradable materials.
Key words: Mg−Ca alloy; directional solidification; microstructure; mechanical properties; degradation performance

1 Introduction

Magnesium (Mg) alloys are expected to be used as biodegradable materials due to their excellent biocompatibility, readily dissolvability, and appropriate elastic modulus, etc [1,2]. It is well known that element Ca plays a critical role in the human body owing to its function in bone construction. Moreover, it has been found that the release of Ca ions into local cellular environments has a positive effect on bone healing [3,4]. Therefore, the element of Ca is considered to be the most suitable alloying element for Mg alloys used as biomedical materials, and extensive efforts have been made to prepare Mg−Ca binary alloys with excellent combination properties of mechanical and degradation properties [5,6]. Although a number of Mg−Ca alloys have been designed and investigated, few Mg−Ca alloys are approved for practical application [7].

The mechanical and degradation properties of the as-cast Mg−Ca alloys are dissatisfactory owing to the coarse microstructure and secondary phase [8]. It is widely accepted that microstructure refinement is an effective way to enhance the combination properties of Mg−Ca alloys. Many manufacturing processes, including rolling and extrusion, etc, have been used to control the microstructure and enhance the combination properties of Mg−Ca alloys [9−11]. SEONG and KIM [9] improved the corrosion resistance of Mg−2Ca and Mg−3Ca alloys by refining the grains and Mg_2Ca phase using high-ratio differential speed rolling. Combined with the post-rolling annealing, the biocorrosion resistance of Mg−Ca alloys with

Corresponding author: Yuan-sheng YANG, Tel: +86-24-23971728, E-mail: ysyang@imr.ac.cn
DOI: 10.1016/S1003-6326(22)66116-8

the grain size of ~6 μm is superior to that of pure Mg. LI et al [10] found that the extrusion speeds greatly affected the mechanical properties of Mg−1.2Ca alloy owing to dynamic recrystallization. Until now, most of the previous studies were concentrated on the properties of wrought Mg−Ca alloys with equiaxed grains, and little attention has been paid to Mg−Ca alloys with columnar grains.

In fact, many Mg alloys with columnar grains have been successfully fabricated by directional solidification, such as Mg−Zn, Mg−Gd, and Mg−Al alloys [12−14]. Microstructure, microsegregation, and mechanical properties of directionally solidified (DSed) Mg alloys have been studied extensively in previous works [15−19]. Little attention has been paid to the investigation of the degradation properties of DSed Mg alloys. Recently, JIA et al [20] reported the degradation behavior of DSed Mg−4Zn alloys in Hank's solution, and they found that directional solidification technology is advantageous in improving the corrosion resistance of Mg alloy. However, there are few studies focused on DSed Mg−Ca alloys for biomedical materials, and there is no experimental assessment of the combination properties of the columnar-structured Mg−Ca alloys.

It has been found that Mg−Ca alloys with the content of Ca ≤1 wt.% exhibit superior mechanical and corrosion properties compared with alloys with higher calcium contents [21]. Therefore, Mg−0.8Ca (wt.%) alloy with different grain morphologies was prepared in this study. The aim of this work is to study the possibility of producing biodegradable DSed Mg−Ca alloys with high strength and high degradation resistance by directional solidification. The microstructure characteristics and combination properties of the DSed Mg−0.8Ca alloys were investigated, and they were compared with the as-cast alloy.

2 Experimental

2.1 Materials and sample preparation

Pure Mg (99.95 wt.%) and Mg−25wt.%Ca master alloy were used to prepare as-cast Mg−0.8Ca alloy. Melting and alloying were performed in a low-carbon steel crucible at 750 °C under an atmosphere of SF_6 (0.8 vol.%) and CO_2 (Bal.). After the raw materials were melted, the melt was stirred for about 3 min to homogenize the alloying elements. Then, the melt was cooled to the pouring temperature of 720 °C before casting into a preheated graphite mold with the dimension of *d*60 mm × 140 mm. Part of the cast ingot was reserved for further tests, and the rest of the cast ingot was machined into *d*6.8 mm cylindrical bars for directional solidification. A directional solidification apparatus with a temperature gradient of 13 °C/mm was used in this work. The bars were placed into alumina crucibles and melted at 900 °C under the protection of Ar followed by pulling down with a rate between 20 to 200 μm/s.

2.2 Microstructure characterization

Specimens, which were taken from the DSed Mg−Ca sample and the cast ingot, were ground to 2.6 μm before polishing and etching with 1 wt.% oxalic solution to reveal their microstructure. A ZEISS Axio Observer.Z1m type optical microscope (OM) and an FEI INSPECT F50 type scanning electron microscope (SEM) were used to observe the microstructure of the specimens. The grain size was measured on the transverse section by the line interception method using ImageJ software. The specimen was ground to 6.5 μm for the XRD test (D8 Advance) to identify the types of phases in the Mg−0.8Ca alloy.

The growth orientation of the DSed Mg−Ca alloy was studied by a Tecnai G20 F30 type transmission electron microscope (TEM) and a TESCAN MAIA3-HKL type electron backscatter diffraction (EBSD). The foils for TEM were taken perpendicular to the growth direction (TD). The crystal orientation was measured from more than five grains for TEM observation. The tested surface for EBSD was the longitudinal section of the DSed samples, and over 10 mm^2 area was scanned in the EBSD test.

2.3 Mechanical properties

Tensile specimens with gauge length of 18 mm and gauge diameter of 3 mm were machined from the DSed samples and the cast ingot. The tensile tests were carried out at a constant speed of 1.0 mm/min by loading along the LD of the DSed samples at room temperature. At least three specimens were tested for each condition. The representative stress−strain curves were given in this work.

2.4 Immersion tests

Cuboid specimens with the dimension of 10 mm × 6 mm × 3 mm were cut from the DSed Mg−Ca samples. The specimens were prepared by mechanical grinding using SiC abrasive papers to 6.5 μm, followed by ultrasonic cleaning in ethanol for 3 min. Immersion tests were conducted in Hank's solution at 37 °C for 48 h. The chemical composition of Hank's solution is given in Table 1. After the immersion test, the specimens were treated by ultrasonic cleaning for 2 min in a solution containing 20% CrO_3 and 1% $AgNO_3$. The specimens before and after the immersion test were weighed using an electronic balance (Sartorius CPA225D) with a precision of 0.01 mg. The corrosion rate R_C (mm/a) can be calculated by the mass loss using [22]

$$R_C=\frac{87600\Delta M}{S\cdot t\cdot\rho} \tag{1}$$

where ΔM is the mass loss (g), S is the exposure area (cm^2), t is the duration of immersion (h), and ρ is the density of Mg−Ca alloy (g/cm^3). Besides, the corrosion morphology was analyzed by SEM before and after the removal of corrosion products. To identify the corrosion products, the corrosion products were analyzed by XRD (D8 Advance).

3 Results and discussion

3.1 Microstructure

The optical micrograph of the as-cast alloy is shown in Fig. 1(a). It can be seen that the microstructure is significantly changed by directional solidification. The grain size of the equiaxed grains in the as-cast alloy is 335 μm, while the grains in the DSed alloys are columnar with parallel trunks, as shown in Figs. 1(b, c). Besides, the grain morphology of the DSed alloys evolves from cellular to dendritic with the increase of the growth rate. Under the growth rate of 20 μm/s, the alloy solidifies with cellular structure with the primary arm spacing of 86 μm, and the microstructure of the transverse section is polygonal. The secondary arms have developed on the side of the columnar grains marked with arrows

Table 1 Chemical composition of Hank's solution (g/L)

NaCl	KCl	$CaCl_2$	$Na_2HPO_4{\cdot}7H_2O$	$MgSO_4{\cdot}7H_2O$	$NaHCO_3$	KH_2PO_4	$C_6H_6O_6$
8	0.4	0.14	0.09	0.2	0.35	0.06	1

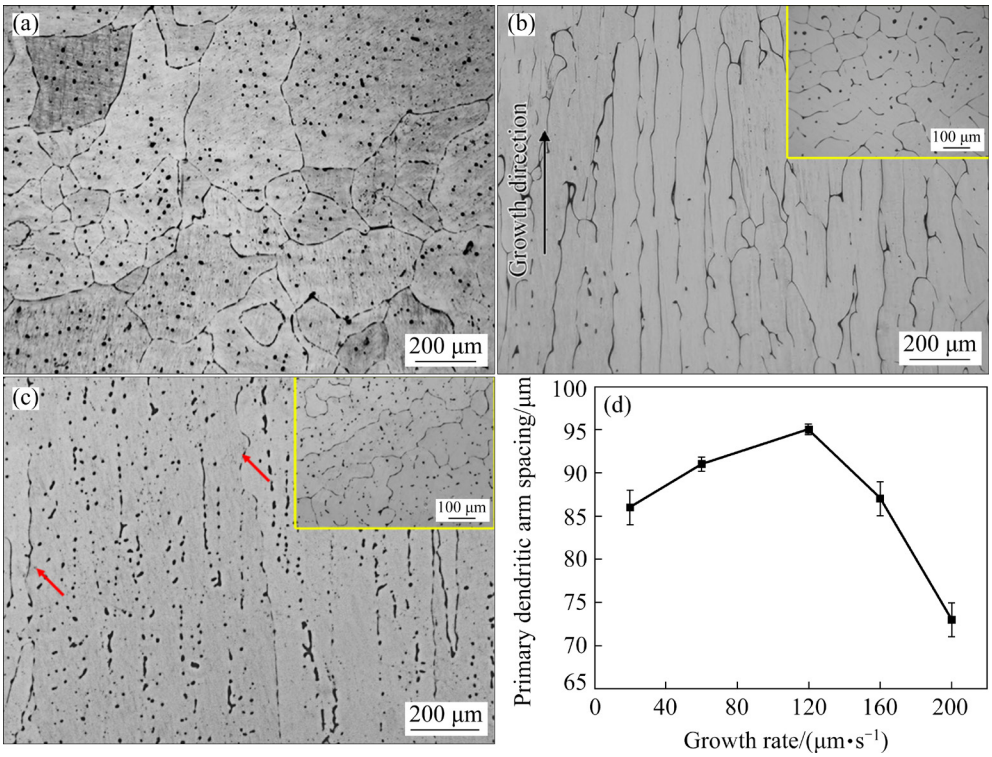

Fig. 1 Micrographs of Mg−0.8Ca alloys (a−c) and primary arm spacing at various growth rates (d): (a) As-cast alloy; (b) DSed alloy with growth rate of 20 μm/s; (c) DSed alloy with growth rate of 160 μm/s

in Fig. 1(c) when the growth rate is increased to 160 μm/s. Besides, the microstructure of the transverse section exhibits a flower shape. The primary arm spacing of the columnar structure at various growth rates is given in Fig. 1(d). It is clear that the primary arm spacing first slightly increases during the transition of the microstructure, and then it decreases with the increase of the growth rate. In addition, the transverse grain boundaries are nearly eliminated by directional solidification compared with the cast ingot. In this work, the alloys with equiaxed structure, cellular structure, and columnar dendritic structure are abbreviated as E-type alloy, C-type alloy, and D-type alloy, respectively.

Based on the experimental findings, the DSed Mg−0.8Ca alloys solidified with the typical columnar structure. KURZ and FISHER [23] have put forward a criterion for the cell-to-dendrite transition, which is expressed as follows:

$$v_{\mathrm{tr}}=\frac{GD}{\Delta T_0 k}=\frac{GD}{mC_0\left(k-1\right)} \tag{2}$$

where v_{tr} is the critical growth rate; G is the temperature gradient; D is the diffusion coefficient in the liquid; ΔT_0 is the temperature interval between the liquidus and solidus; m is the liquidus slope; k is the equilibrium partition coefficient and C_0 is the initial alloy composition. These parameters of Mg−0.8Ca alloy are listed in Table 2 [24]. In this case, the calculation result of v_{tr} is 30 μm/s, which indicates that the alloy will solidify with cellular structure at the growth rate slower than 30 μm/s. The calculated result is consistent with the experimental result in this study. After the structure evolves from cellular to dendritic, the primary arm spacing slightly rises. This phenomenon has been reported in many researches of DSed alloys [25,26]. It can be attributed to the change of the tip radius affected by the appearance of the secondary dendritic arm.

Table 2 Parameters for DSed Mg−0.8Ca

Parameter	Value
G/(K·mm^{-1})	13
D/(m^2·s^{-1})	2.19×10^{-8}
m/(K·wt.%$^{-1}$)	−12.67
C_0/wt.%	0.8
k	0.06

The distribution and morphology of the secondary phases in the as-cast alloy and DSed alloys are observed by SEM under the backscattering mode, as displayed in Fig. 2. The secondary phases are mainly distributed inside and between the equiaxed grains existing as eutectics for E-type alloy, while they are mainly distributed along the grain boundaries for the C-type and D-type alloys. Besides, the secondary phases in D-type alloy are much finer and more dispersed along the grain boundaries. Apparently, the volume fraction of the secondary phases for the C-type alloy is less than that of the E-type and D-type alloys. In addition, as Figs. 2(b, e) show, the eutectic morphology of the C-type alloy is different from that of the as-cast alloy. The results of EDS show that the eutectic phase mainly consists of elements of Mg and Ca, as displayed in Figs. 2(b, f). Combined with the phase diagram analysis and the XRD diffraction pattern (Fig. 3) [27], it can be known that the eutectic phase in Mg−0.8Ca alloys is α-Mg/Mg_2Ca.

To investigate the growth orientation of the DSed Mg−0.8Ca alloys, the selected area electron diffraction (SAED) pattern was taken, as shown in Fig. 4. It can be known that the preferred crystal growth orientation for the DSed alloy is $\langle 11\bar{2}0\rangle$ from the SAED pattern. EBSD was used to further identify the growth orientation as well. The orientation map and the X-direction of inverse pole figures obtained by EBSD are presented in Figs. 5(a, b). The results show that most of the grains grow along with $\langle 11\bar{2}0\rangle$ and expose {0002} outside, which is consistent with the result of TEM. The same preferred growth orientation of Mg alloys has been reported by JIA et al [16] and SHUAI et al [18]. The grain size detected by EBSD is very large due to the fact that one grain contains many columnar grains with similar orientation. Besides, it can be recognized from Fig. 5(c) that most of the grain boundaries are low angle grain boundaries.

It is well accepted that the grains generally prefer to grow along those directions perpendicular to the crystallographic planes with higher surface energy [28]. Some previous works have confirmed that the closest packed crystal plane {0001} has the lowest interfacial energy, which means that the {0001} plane prefers to wrap the outside of the grains during the solidification [29,30]. Besides, the directions perpendicular to the {0001} plane have

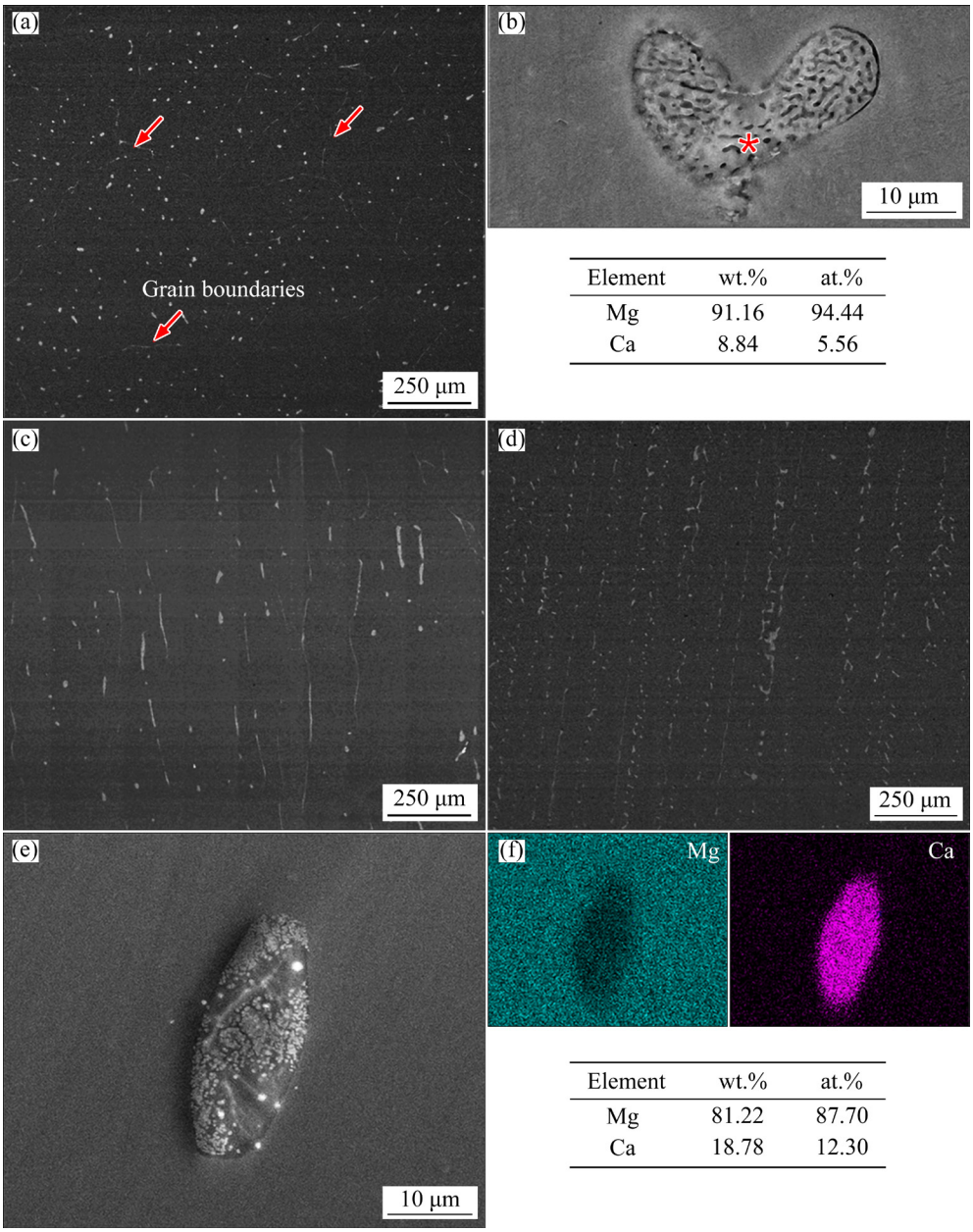

Fig. 2 Distribution and morphology of secondary phases in E-type alloy (a, b), C-type alloy (c), D-type alloy (d), and eutectic phase in C-type alloy (e) with EDS results (f)

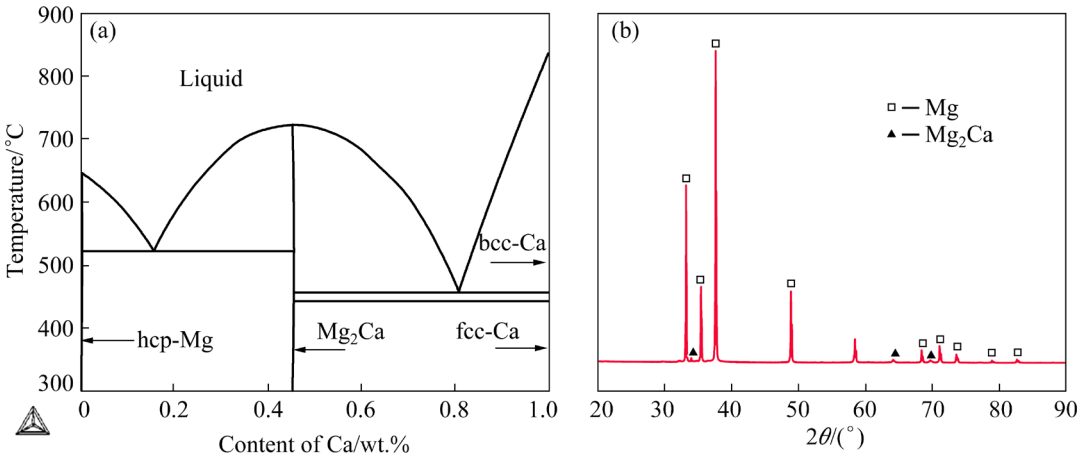

Fig. 3 Phase diagram of Mg−Ca alloy (a) [27] and XRD diffraction pattern of Mg−0.8Ca alloy (b)

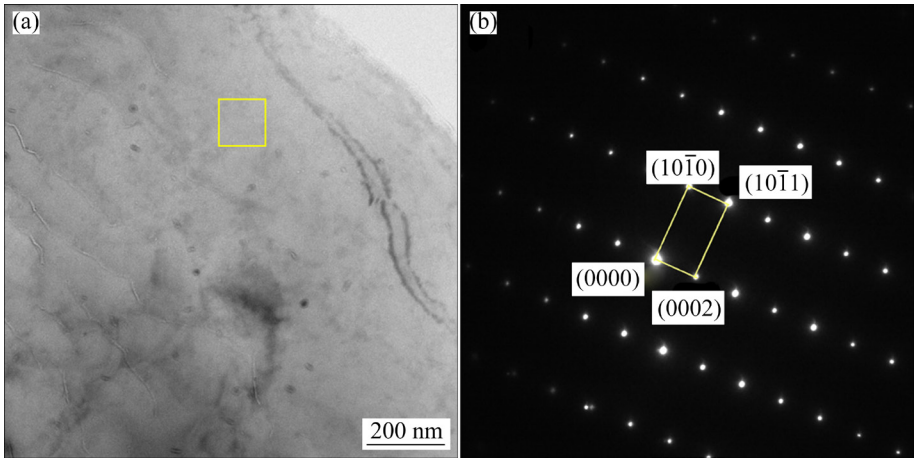

Fig. 4 SAED pattern from growth direction of DSed Mg−0.8Ca alloy

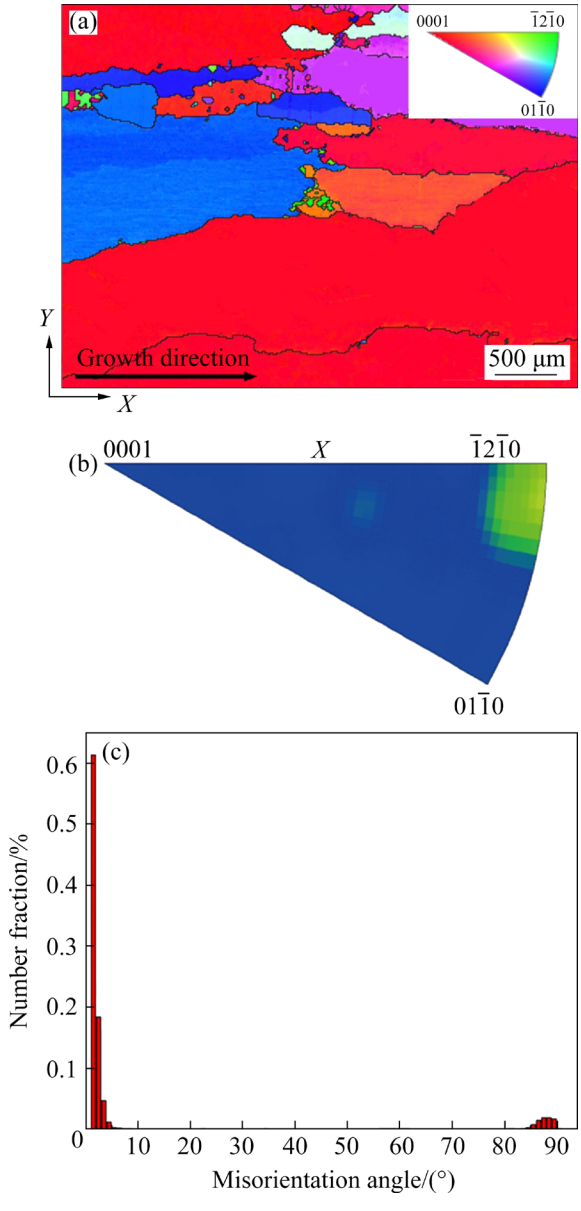

Fig. 5 EBSD orientation map of *X*-direction (a), *X*-direction of inverse pole figures (b), and misorientation angle distributions of DSed Mg−0.8Ca alloy (c)

the lowest growth rate based on the Bravais rule. For HCP Mg alloys, ⟨11$\bar{2}$0⟩ is one of the orientations on the basal plane, and the surface energy of {11$\bar{2}$0} is higher than that of many other crystal orientations, including {0001}, {10$\bar{1}$0} and {10$\bar{1}$1} [28]. In other words, crystal growth along ⟨11$\bar{2}$0⟩ conforms to the energy selection for crystal growth. Therefore, it is reasonable that the crystal grows with ⟨11$\bar{2}$0⟩ orientation.

3.2 Mechanical properties

The tensile stress−strain curves of the experimental alloys are shown in Fig. 6. The results indicate that the solidification condition strongly affects the mechanical properties of Mg−Ca alloys. For the E-type alloy, the tensile yield strength (TYS), ultimate tensile strength (UTS), and elongation (EL) are 55 MPa, 89 MPa, and 2%, respectively. After the directional solidification, the mechanical properties of Mg−0.8Ca alloys are

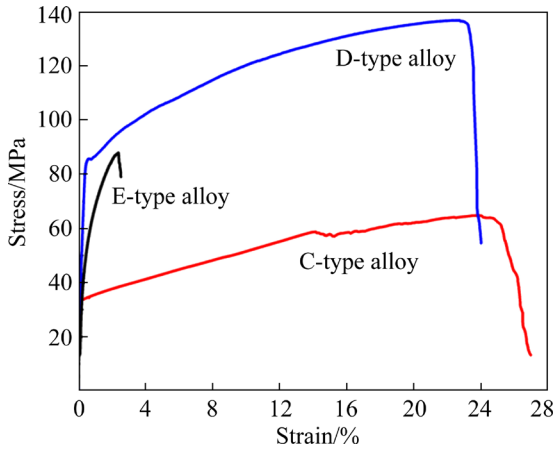

Fig. 6 Tensile stress−strain curves of Mg−0.8Ca alloys with different microstructures

significantly improved, especially for the EL. The TYS, UTS, and EL of C-type alloy are 33 MPa, 64 MPa, and 27%, respectively, and those of the D-type alloy are 86 MPa, 137 MPa, and 24%, respectively. The TYS and UTS of the C-type alloy are smaller than that of the E-type alloy, while the EL of the C-type alloy is 13.5 times that of the E-type alloy. As for the D-type alloy, its tensile strength and ductility are superior to those of the E-type and C-type alloys. The TYS, UTS, and EL of the D-type alloy are 1.6 times, 1.5 times, and 12 times those of the E-type alloy, respectively. The results of the mechanical properties demonstrate that the mechanical strength and ductility of the Mg−Ca alloy can be greatly enhanced by directional solidification.

Figure 7 shows the fracture micrographs of the experimental alloys. It can be seen that the cracks across the grains for both two alloys, but the cracks also extend along the grain boundaries of the E-type alloy marked with the arrow in Fig. 7(a). The fracture morphologies are presented in Fig. 8. It is noted that the type of fracture is different between the E-type alloy and the DSed alloys. As Fig. 8(a) shows, the edges of the fracture are sharp, and river patterns and holes with coarse particle phases inside can be observed for the E-type alloy, indicating the brittle fracture. However, there are abundant dimples and river patterns on the fracture surface of DSed alloy, meaning a mixed fracture of microvoid coalescence and cleavage fracture.

The results show that the ductility of Mg−Ca alloy can be greatly improved by the directional solidification, and the mechanical strength of the

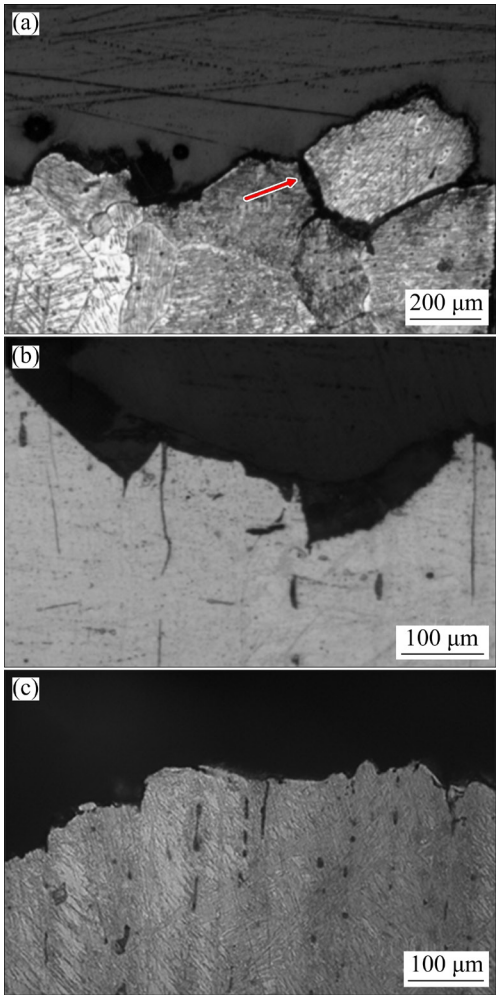

Fig. 7 Fracture micrographs observed by OM: (a) E-type alloy; (b) C-type alloy; (c) D-type alloy

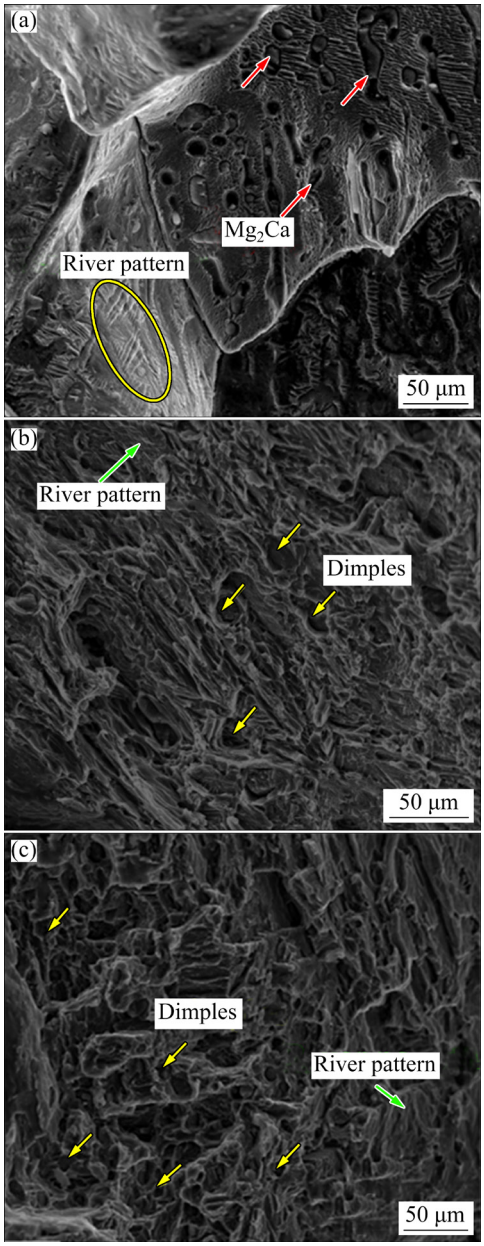

Fig. 8 SEM images of fracture morphology: (a) E-type alloy; (b) C-type alloy; (c) D-type alloy

D-type alloy is much higher than that of E-type alloy. However, the mechanical strength of the C-type alloy is lower than that of the E-type alloy owing to the type of grain boundaries and the distribution of the eutectic phase. The grain boundaries of the C-type alloy are the small-angle grain boundaries due to the similar crystal orientation of the cellular grains (Fig. 5(c)). Although the primary arm spacing of the C-type alloy is much less than the grain size of the E-type alloy, the large-angle grain boundaries in the E-type alloy hinder the movement of dislocations during the deformation more effectively than the small-angle grain boundaries in the C-type alloy. Therefore, in this respect, the low angle grain boundaries of the C-type alloy lead to a drop in mechanical strength. Besides, the Mg_2Ca phases with different crystal structures from α-Mg impede the movement of dislocations as well. Compared with the C-type alloy, the large volume fraction of the Mg_2Ca phase in the E-type alloy leads to the enhancement of the strength as well.

As for the EL, the stress concentration caused by the coarse Mg_2Ca phase in the E-type alloy and the bad deformation coordination caused by the random crystal orientation of the grains in the E-type alloy are the key factors that decrease the ductility of Mg alloys. Moreover, cracks are easy to extend along the grain boundaries of the E-type alloy as Fig. 7(a) shows. However, columnar grains with a similar crystal orientation make contributions to the coordinated deformation for the DSed alloys. At the same time, less Mg_2Ca phase distributed along the grain boundaries is also helpful to avoid the stress concentration. Therefore, it is hard for the cracks to extend along the columnar grain boundaries. A schematic diagram of the extension of the crack is displayed in Fig. 9.

It is worth noting that the mechanical strength of the D-type alloy is larger than that of E-type and C-type alloys. As Fig. 2 shows, the eutectic phases in the D-type alloy are much finer than the phase in E-type and C-type alloys, and the eutectic phases are dispersedly distributed in the D-type alloy. It is well known that the refined and dispersed secondary phase can effectively improve the mechanical properties of the Mg alloy. Consequently, both the mechanical strength and ductility of the D-type alloy are outstanding.

Figure 10 presents the mechanical properties of several kinds of Mg−Ca alloys [8,11,31,32]. The mechanical strength of Mg−Ca alloy can be dramatically enhanced by rolling or extrusion, and the EL can reach 20%. However, the DSed Mg−Ca alloy exhibits ultrahigh EL larger than 20%, and its mechanical strength can be improved by adjusting the growth rate, which has great potential to be used as biomaterials.

3.3 Degradation performance

3.3.1 Immersion test

Figure 11 shows the results of the immersion test in Hank's solution for 48 h including the mass loss and the corresponding corrosion rate. Apparently, the degradation rate of Mg−0.8Ca alloy can be significantly decreased using directional solidification. The degradation rates of the C-type and D-type alloys are almost half that of the E-type alloy. The degradation rates of the C-type and D-type alloys are 2.54 and 2.37 mm/a, respectively, indicating the better corrosion resistance of the D-type alloy.

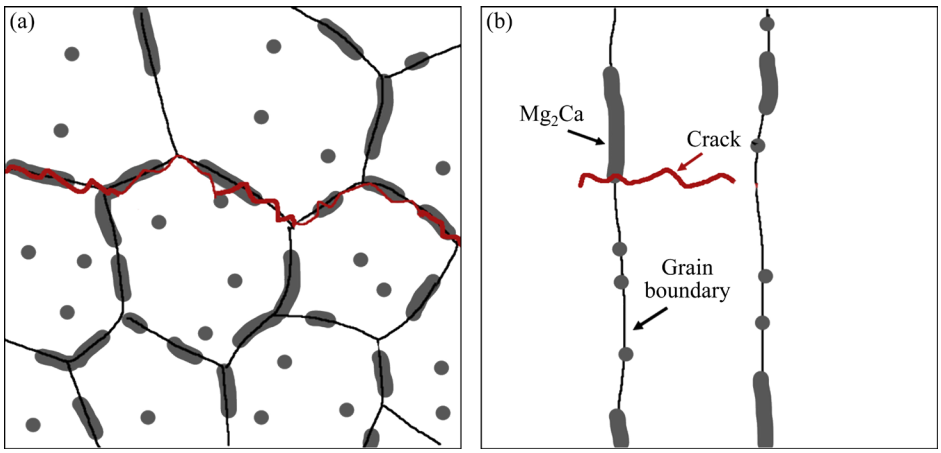

Fig. 9 Schematic diagram of extension of crack of Mg−Ca alloys: (a) E-type alloy; (b) DSed alloy

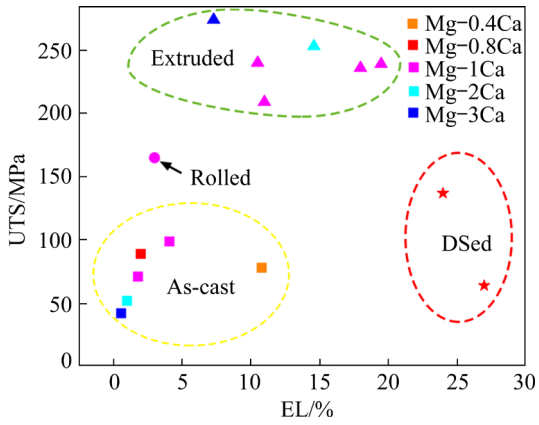

Fig. 10 Mechanical properties of several kinds of Mg−Ca alloys [8,11,31,32]

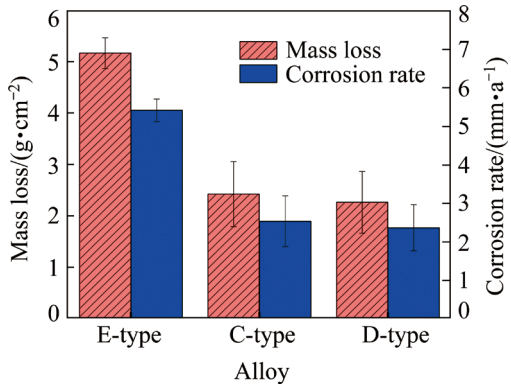

Fig. 11 Results of immersion test in Hank's solution for 48 h

3.3.2 Corrosion morphology

The corrosion morphologies of the Mg−Ca alloys are shown in Fig. 12. It can be seen in Figs. 12(a, b) that the surface of the E-type specimen has been totally covered with the corrosion products after the immersion for 48 h, while a large area of the surfaces of the DSed specimens is just slightly corroded (Figs. 12(c−f)). Additionally, the corrosion products are mainly distributed along the grain boundaries drawing the outline of the equiaxed grain for the E-type specimen, as inserted in Fig. 12(a).

As for the C-type and D-type alloys, the corrosion products mainly pile up as lines parallel with the growth direction. Besides, it can be seen in Figs. 12(a, b) that the corrosion products do not fully cover the surface of the E-type specimen, which means that the corrosion product film (CPF) cannot provide effective protection. However, the C-type and D-type specimens have an intact CPF compared with the E-type specimen. Moreover, the CPF of the D-type is much solid and compact than that of the C-type specimen. The EDS results in Fig. 12(f) show that the CPF contains elements of O, Mg, P, and Ca. The XRD pattern of the corrosion products is shown in Fig. 13, and the result shows that the corrosion products mainly consist of $Mg(OH)_2$, $(Ca,Mg)_3(PO_4)_2$, and hydroxyapatite (HA).

The corrosion morphologies after the removal of the corrosion products of the experimental alloys are presented in Fig. 14. Deep holes with a dimension of 1 mm in diameter can be observed on the specimen of the E-type alloy, which should be caused by the peeling-off of some large equiaxed grains, as marked by the arrow in Fig. 14(a). On the contrary, the DSed alloys experience more uniform and slight corrosion with relatively flat corrosion morphology compared with the E-type alloy. Among the DSed alloys, it can be observed in Figs. 14(b, c) that the D-type alloy has suffered a slighter corrosion attack than the C-type alloy.

3.3.3 Corrosion resistance

The results of the immersion test show that the corrosion resistance of the DSed alloys is better than that of the E-type alloy. For Mg−Ca alloys, the Mg_2Ca phases act as anodes and the Mg matrix as the cathode during the corrosion, which leads to microgalvanic corrosion [33]. For the as-cast Mg−0.8Ca alloy, the Mg_2Ca phases are mainly distributed on the grain boundaries. Therefore, the corrosion proceeding along the equiaxed grain of the E-type alloy eventually results in the grain shedding, as shown in Fig. 14(a). However, the DSed alloys with Mg_2Ca discontinuous distributed on the grain boundaries can effectively avoid the grain falling-off due to its long grain boundaries, which is helpful to enhance the corrosion resistance of the Mg−Ca alloy. A schematic diagram of the corrosion mechanism of E-type and DSed alloy is presented in Fig. 15. At the same time, Mg_2Ca phase exists in the as-cast alloy as typical lamellar eutectic, which will increase the contact area between the anode and cathode and accelerate the corrosion rate. Besides, it is well known that there is a potential difference between the grains with different crystal orientations, which will result in microgalvanic corrosion [34]. In this study, the grains of the E-type alloy are randomly orientated, while the grains of the DSed alloys have a similar crystal orientation. Therefore, the microgalvanic

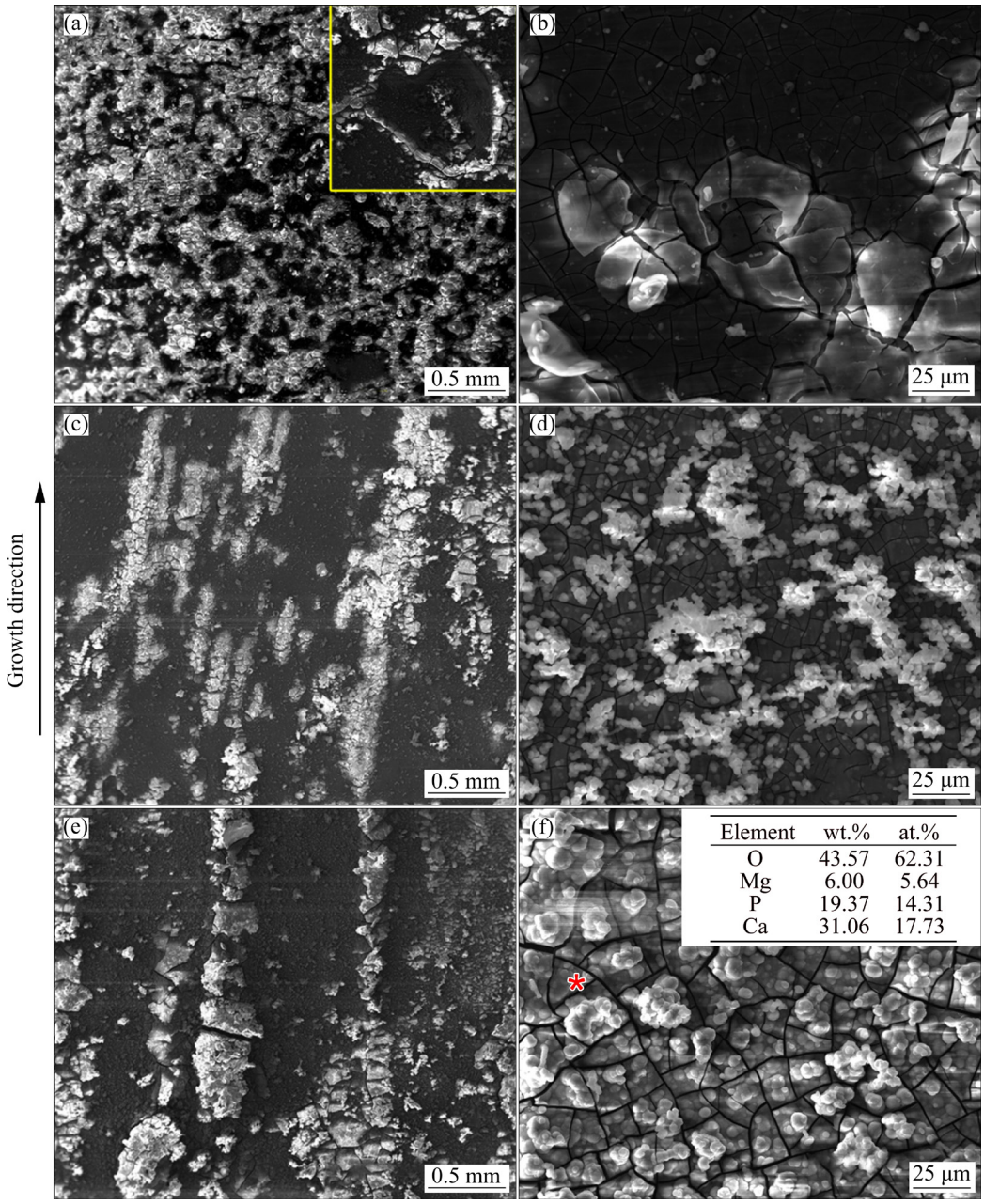

Fig. 12 Corrosion morphologies of E-type alloy (a, b), C-type alloy (c, d) and D-type alloy (e, f)

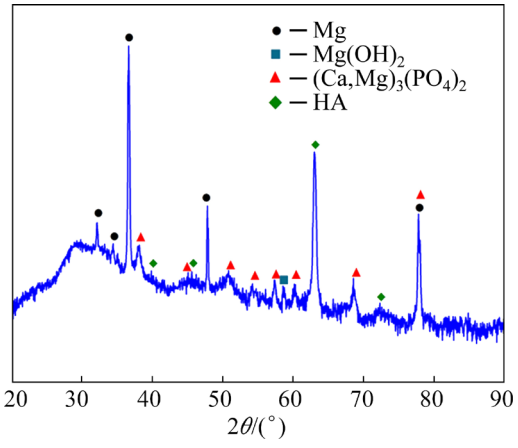

Fig. 13 XRD pattern of corrosion products

corrosion caused by different orientations of grains is greatly avoided by directional solidification. As discussed above, the superior corrosion resistance of the DSed alloys is beneficial from the columnar grains with similar orientations.

Among the three experimental alloys, the corrosion resistance of the D-type alloy is the best. In fact, the fine microstructure and dispersed distribution of Mg_2Ca phases for the D-type alloy promote the formation of a compact and protective CPF during the corrosion, improving the corrosion resistance of the Mg−Ca alloy. Therefore, the D-type alloy exhibits excellent corrosion resistance

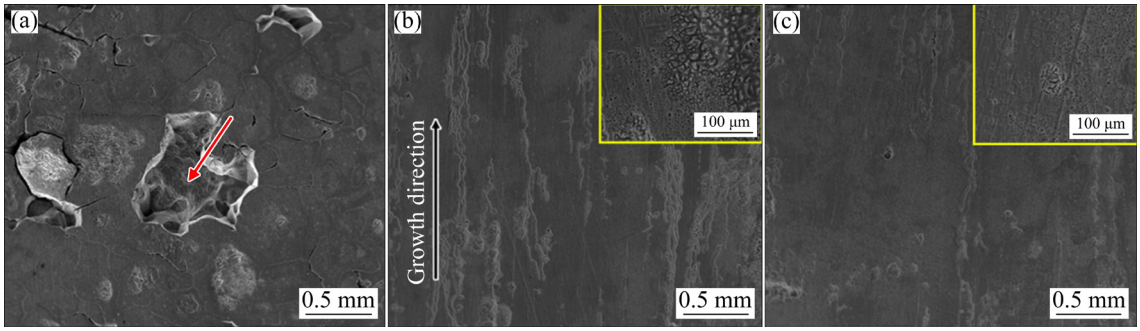

Fig. 14 Corrosion morphologies after removal of corrosion products: (a) E-type alloy; (b) C-type alloy; (c) D-type alloy

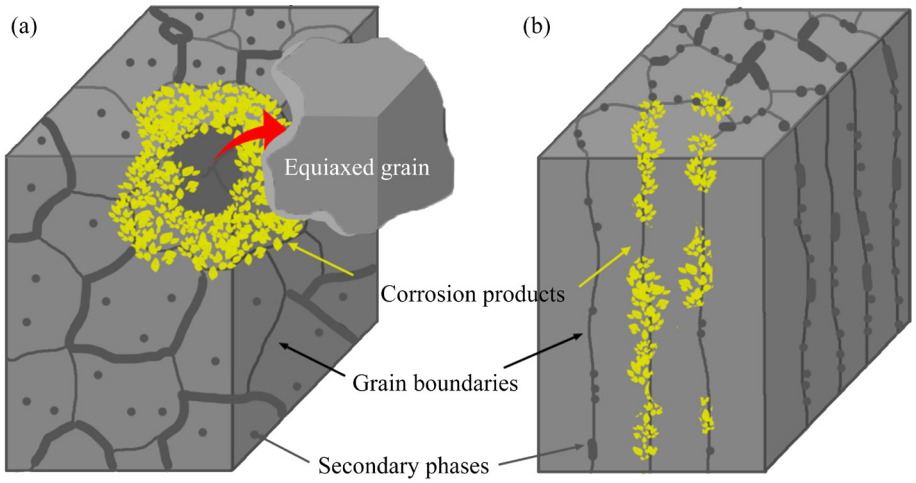

Fig. 15 Schematic diagram of corrosion mechanism of E-type alloy (a) and DSed alloy (b)

in Hank's solution due to the formation of a protective CPF. Table 3 summarizes in vitro corrosion rates of various Mg−Ca alloys. It can be seen that the corrosion resistance of DSed Mg−0.8Ca alloys is better than that of many as-cast Mg−Ca alloys and even better than that of as-extruded Mg−Ca alloys. The DSed Mg−0.8Ca alloy shows great potential for application as a biodegradable material.

Table 3 Summary of in vitro corrosion rates of various Mg−Ca alloys

Alloy	State	Medium	Corrosion rate/ ($mm \cdot a^{-1}$)	Ref.
Mg−0.8Ca	DSed	Hank's	2.37	−
Mg−0.8Ca	DSed	Hank's	2.54	−
Mg−0.66Ca	As-cast	SBF	7.00	[6]
Mg−0.54Ca	As-extruded	Hank's	5.76	[35]
Mg−0.79Ca	As-extruded	Hank's	2.76	[35]
Mg−2Ca	As-cast	Kokubo	6.89	[36]
Mg−4Ca	As-cast	Kokubo	9.04	[36]

4 Conclusions

(1) The columnar-structured Mg−Ca alloys were successfully fabricated by directional solidification. With the increase of growth rate, the microstructure evolves from cellular to dendritic. The microstructure evolution is well in accordance with the criterion put forward by Kurz and Fisher.

(2) The DSed Mg-Ca alloys have a $\langle 11\bar{2}0\rangle\{0002\}$ texture along the growth direction, which is governed by the interfacial energy and related crystallographic anisotropy.

(3) The mechanical properties can be significantly improved by directional solidification compared with the E-type alloy. Using directional solidification can effectively solve the problem of brittle fracture of the as-cast Mg−Ca alloy, and the EL of the DSed Mg−Ca alloy can exceed 20%. The mechanical strength of the DSed alloy can be improved by adjusting the growth rate.

(4) The corrosion resistance of the Mg−Ca alloy is greatly enhanced by the directional

solidification, and the corrosion resistance of the D-type alloy is the best among the experimental alloys. The D-type alloy can produce a protective CPF and avoid grain shedding during the degradation due to its fine columnar grains with similar orientation.

(5) The D-type alloy with superior mechanical and degradation properties shows great potential to be used as biodegradable material.

Acknowledgments

This work was supported by the Key Research and Development Plan of Shandong Province, China (No. 2019JZZY020329), the National Key Research and Development Program of China (No. 2017YFB0103904), the National Natural Science Foundation of China (No. 51701211), and Dongguan Innovative Research Team Program, China (No. 2020607134012).

References

[1] BOMMALA V K, KRISHNA M G, RAO C T. Magnesium matrix composites for biomedical applications: A review [J]. Journal of Magnesium and Alloys, 2019, 7: 72−79.

[2] TIAN Yuan, MIAO Hong-wei, NIU Jia-lin, HUANG Hua, KANG Bin, ZENG Hui, DING Wen-jiang, YUAN Guang-yin. Effects of annealing on mechanical properties and degradation behavior of biodegradable JDBM magnesium alloy wires [J]. Transactions of Nonferrous Metals Society of China, 2021, 31: 2615−2625.

[3] XIA Yu, WU Liang, YAO Wen-hui, HAO Meng, CHEN Jing, ZHANG Cheng, WU Tao, XIE Zhi-hui, SONG Jiang-feng, JIANG Bin, MA Yan-long, PAN Fu-sheng. In-situ layered double hydroxides on Mg−Ca alloy: Role of calcium in magnesium alloy [J]. Transactions of Nonferrous Metals Society of China, 2021, 31: 1612−1627.

[4] LIU Bao-sheng, CAO Miao-miao, ZHANG Yue-zhong, HU Yong, GONG Chang-wei, HOU Li-feng, WEI Ying-hui. Microstructure, anticorrosion, biocompatibility and anti-bacterial activities of extruded Mg−Zn−Mn strengthened with Ca [J]. Transactions of Nonferrous Metals Society of China, 2021, 31: 358−370.

[5] LIN P C, LIN K F, CHIU C, SEMENOV V I, LIN H C, CHEN M J. Effect of atomic layer plasma treatment on TALD-ZrO_2 film to improve the corrosion protection of Mg−Ca alloy [J]. Surface and Coatings Technology, 2021, 427: 127811.

[6] NIKHIL T T, SHEBEER A R, JOSEPH M A, HANAS T. In vitro biodegradation and biomineralization of Mg−Ca alloys [J]. Materials Today: Proceedings, 2020, 22: 2870−2876.

[7] SEKAR P, NARENDRANATH S, DESAI V. Recent progress in in vivo studies and clinical applications of magnesium based biodegradable implants—A review [J]. Journal of Magnesium and Alloys, 2021, 9: 1147−1163.

[8] GU Xu-nan, LOU Si-quan, ZHENG Yu-feng. The development of binary Mg−Ca alloys for use as biodegradable materials within bone [J]. Biomaterials, 2008, 29: 1329−1344.

[9] SEONG J W, KIM W J. Development of biodegradable Mg−Ca alloy sheets with enhanced strength and corrosion properties through the refinement and uniform dispersion of the Mg_2Ca phase by high-ratio differential speed rolling [J]. Acta Biomaterialia, 2015, 11: 531−542.

[10] LI Jing-ren, ZHANG Ai-yue, PAN Hu-cheng, REN Yu-ping, ZENG Zhuo-ran, HUANG Qiu-yan, YANG Chang-lin, MA Li-feng, QIN Gao-wu. Effect of extrusion speed on microstructure and mechanical properties of the Mg−Ca binary alloy [J]. Journal of Magnesium and Alloys, 2020, 9: 1297−1303.

[11] PAN Hu-cheng, YANG Chang-lin, YANG Yan-tao, DAI Yong-qiang, ZHOU Deng-shan, CHAI Lin-jiang, HUANG Qiu-yan, YANG Qing-shan, LIU Sheng-ming, REN Yu-ping, QIN Gao-wu. Ultra-fine grain size and exceptionally high strength in dilute Mg−Ca alloys achieved by conventional one-step extrusion [J]. Materials Letters, 2019, 237: 65−68.

[12] WANG Yong-biao, JIA Sen-sen, WEI Ming-guang, PENG Li-ming, WU Yu-juan, JI Yan-zhou, CHEN Long-Qing, LIU Xin-tian. Coupling in situ synchrotron X-ray radiography and phase-field simulation to study the effect of low cooling rates on dendrite morphology during directional solidification in Mg−Gd alloys [J]. Journal of Alloys and Compounds, 2020, 815: 152385.

[13] ZHAO Sheng-shi, LIN Xiao-ping, DONG Yun, NIU Yi, XU Dan, SUN Heng. High-temperature tensile properties and deformation mechanism of polycrystalline magnesium alloys with specifically oriented columnar grain structures [J]. Materials Science and Engineering A, 2018, 729: 300−309.

[14] WANG Jia-he, YANG Guang-yu, LIU Shao-jun, JIE Wan-qi. Microstructure and room temperature mechanical properties of directionally solidified Mg−2.35Gd magnesium alloy [J]. Transactions of Nonferrous Metals Society of China, 2016, 26: 1294−1300.

[15] FANG D R, ZHAO S S, LIN X P, CHAI T, KUO Y, SUN H, DONG Y. Correlation between microstructure and mechanical properties of columnar crystals in the directionally solidified Mg−Gd−Y−Er alloy [J]. Journal of Magnesium and Alloys, 2021. https://doi.org/10.1016/j.jma.2020.11.025.

[16] JIA Hong-min, FENG Xiao-hui, YANG Yuan-sheng. Microstructure evolution and growth orientation of directionally solidified Mg−4wt.%Zn Alloy with different growth rates [J]. Acta Metallurgica Sinica (English Letter), 2017, 30: 1185−1191.

[17] LIU Shao-jun, YANG Guang-yu, JIE Wan-qi. Microstructure, microsegregation, and mechanical properties of directional solidified Mg−3.0Nd−1.5Gd alloy [J]. Acta Metallurgica. Sinica (English Letter), 2014, 27: 1134−1143.

[18] SHUAI San-san, GUO En-yu, ZHENG Qi-wei, WANG Ming-yue, JING Tao. Characterisation of three-dimensional dendritic morphology and orientation selection of α-Mg in Mg−Ca alloy using synchrotron X-ray tomography [J]. Materials Characterization, 2016, 111: 170−176.

[19] JIA Hong-min, FENG Xiao-hui, YANG Yuan-sheng. The mechanical anisotropy of directionally solidified Mg−4wt.%Zn alloy under compression test [J]. Materials Science and Engineering A, 2019, 762: 138104.

[20] JIA Hong-min, FENG Xiao-hui, YANG Yuan-sheng. Effect of grain morphology on the degradation behavior of

Mg−4wt.%Zn alloy in Hank's solution [J]. Materials Science and Engineering C, 2020, 106: 110013.
[21] SEONG J W, KIM W J. Mg−Ca binary alloy sheets with Ca contents of ≤1 wt.% with high corrosion resistance and high toughness [J]. Corrosion Science, 2015, 98: 372−381.
[22] WANG Xue-jian, CHEN Zong-ning, ZHANG Yu-bo, GUO En-yu, KANG Hui-jun, HAN Pei, WANG Tong-min. Influence of microstructural characteristics on corrosion behavior of Mg–5Sn–3In alloy in Hank's solution [J]. Transactions of Nonferrous Metals Society of China, 2021, 31: 2999−3011.
[23] KURZ W, FISHER D J. Fundamentals of solidification [M]. Trans Tech Publications, 1992.
[24] CHEN Yong-jun, XU Zhi-gang, SMITH C, SANKAR J. Recent advances on the development of magnesium alloys for biodegradable implants [J]. Acta Biomaterialia, 2014, 10: 4561−4573.
[25] PALIWAL M, JUNG I H. The evolution of the growth morphology in Mg−Al alloys depending on the cooling rate during solidification [J]. Acta Materialia, 2013, 61: 4848−4860.
[26] MIYATA Y, SUZUKI T, UNO J I. Cellular and dendritic growth. Part I: Experiment [J]. Metallurgical Transactions A, 1985, 16: 1799−1805.
[27] BRUBAKER C O, LIU Z K. A computational thermodynamic model of the Ca−Mg−Zn system [J]. Journal of Alloys and Compounds, 2004, 370: 114−122.
[28] DU Jiang-lian, GUO Zhi-peng, ZHANG Ang, YANG Man-hong, LI Mei, XIONG Shou-mei. Correlation between crystallographic anisotropy and dendritic orientation selection of binary magnesium alloys [J]. Scientific Reports, 2017, 7: 13600.
[29] DU Jing-lian, ZHANG Ang, GUO Zhi-peng, YANG Man-hong, LI Mei, LIU Feng, XIONG Shou-mei. Effect of additional solute elements (X = Al, Ca, Y, Ba, Sn, Gd and Zn) on crystallographic anisotropy during the dendritic growth of magnesium alloys [J]. Journal of Alloys and Compounds, 2019, 775: 322−329.
[30] CHANG Guo-wei, CHEN Shu-ying, ZHOU Cong, YUE Xu-dong, QI Yi-hui. Relationship between solid/liquid interface and crystal orientation for pure magnesium solidified in fashion of cellular crystal [J]. Transactions of Nonferrous Metals Society of China, 2010, 20: 289−293.
[31] JEONG Y S, KIM W J. Enhancement of mechanical properties and corrosion resistance of Mg−Ca alloys through microstructural refinement by indirect extrusion [J]. Corrosion Science, 2014, 82: 392−403.
[32] SHE J, ZHOU S B, PENG P, TANG A T, WANG Y, PAN H C, YANG C L, PAN F S. Improvement of strength-ductility balance by Mn addition in Mg−Ca extruded alloy [J]. Materials Science and Engineering A, 2020, 772: 138796.
[33] GONG Chang-wei, HE Xin-ze, FANG Da-qing, LIU Bao-sheng, YAN Xue. Effect of second phases on discharge properties and corrosion behaviors of the Mg−Ca−Zn anodes for primary Mg−air batteries [J]. Journal of Alloys and Compounds, 2021, 861: 158493.
[34] WANG Yu-jiao, ZHANG Yun, JIANG Hai-tao. Effect of grain size uniformity and crystallographic orientation on the corrosion behavior of Mg−2Zn−1Al bar [J]. Materials Characterization, 2021, 179: 111374.
[35] CUI Lan-yue, ZENG Rong-chang, GUAN Shao-kang, QI Wei-chen, ZHANG Fen, LI Shuo-qi, HAN En-hou. Degradation mechanism of micro-arc oxidation coatings on biodegradable Mg−Ca alloys: The influence of porosity [J]. Journal of Alloys and Compounds, 2017, 695: 2464−2476.
[36] BAKHSHESHI-RAD H R, IDRIS M H, ABDUL-KADIR M R, OURDJINI A, MEDRAJ M, DAROONPARVAR M, HAMZAH E. Mechanical and bio-corrosion properties of quaternary Mg−Ca−Mn−Zn alloys compared with binary Mg−Ca alloys [J]. Materials & Design, 2014, 53: 283−292.

利用定向凝固方法提高 Mg−0.8%Ca 合金的力学性能和降解性能

张 一[1,2]，冯小辉[1]，黄秋燕[1]，李应举[1]，杨院生[1,2]

1. 中国科学院 金属研究所，沈阳 110016；
2. 中国科学技术大学 材料科学与工程学院，沈阳 110016

摘 要：研究定向凝固 Mg−0.8Ca(质量分数，%)合金的力学性能以及在 Hank's 溶液中的降解性能，并与普通铸造 Mg−0.8Ca 合金的性能进行比较。利用 OM、SEM、TEM 和 EBSD 对定向凝固合金的显微组织进行研究。结果表明，定向凝固合金具有柱状晶组织，且合金的柱状晶粒沿 $\langle 11\bar{2}0\rangle$ 方向择优生长。与普通的铸造合金相比，定向凝固 Mg−0.8Ca 合金的强度和塑性均显著提高。同时，定向凝固 Mg−0.8Ca 合金在 Hank's 溶液中的抗腐蚀能力也得到极大提升。合金在 Hank's 溶液中主要发生微电偶腐蚀，合金的腐蚀产物包括 $Mg(OH)_2$、$(Ca,Mg)_3(PO_4)_2$ 和羟基磷灰石。定向凝固合金性能的提高主要与柱状晶组织特征及共晶的再分布有关。具有柱状树枝晶组织的定向凝固 Mg−0.8Ca 合金有望用作可降解生物医用材料。

关键词：Mg−Ca 合金；定向凝固；显微组织；力学性能；降解性能

(Edited by Bing YANG)